

## Article

# Tuning the Piezoelectric Performance of $K_{0.5}Na_{0.5}NbO_3$ through Li Doping: Insights from Structural, Elastic and Electronic Analyses

Hui Li \*, Tianxiang Zhou, Kang Xu, Han Wang, Wenke Lu and Jinyi Liu

School of Materials Science and Engineering, Chang'an University, Xi'an 710064, China; zhou\_tx@chd.edu.cn (T.Z.); xk11252024@163.com (K.X.); 2023131021@chd.edu.cn (H.W.); luwenke420@gmail.com (W.L.); liujinyi\_99@163.com (J.L.)

\* Correspondence: huili128@gmail.com; Tel./Fax: +86-29-82337340

**Abstract:** The structural, elastic, piezoelectric, and electronic properties of Li-doped  $K_{0.5}Na_{0.5}NbO_3$  ( $K_{0.5-x}Na_{0.5-y}Li_{x+y}NbO_3$ , KNN-L) are calculated. The properties of KNN-L are related to the Li-doping content and the replaced K or Na atoms. The bulk modulus, the shear modulus, and Young's modulus of KNN-L are mostly higher than those of KNN, and the hardness value increases. The Poisson ratio of KNN-L is lower than that of most KNN, and the ductility is reduced. All doped structures are direct band gap semiconductors.  $K_{0.5}Na_{0.375}Li_{0.125}NbO_3$  has the largest piezoelectric charge constant,  $d_{33} = 44.72$  pC/N, in the respective structures, which is 1.5 fold that of  $K_{0.5}Na_{0.5}NbO_3$  (29.15 pC/N). The excellent piezoelectric performance of Li-doping KNN-L was analyzed from the insights of elastic and electronic properties.

**Keywords:** Li-doped  $K_{0.5}Na_{0.5}NbO_3$ ; elastic properties; electronic properties; piezoelectric properties; first-principles



**Citation:** Li, H.; Zhou, T.; Xu, K.; Wang, H.; Lu, W.; Liu, J. Tuning the Piezoelectric Performance of  $K_{0.5}Na_{0.5}NbO_3$  through Li Doping: Insights from Structural, Elastic and Electronic Analyses. *Materials* **2024**, *17*, 2118. <https://doi.org/10.3390/ma17092118>

Academic Editor: José Luis Gómez Ribelles

Received: 29 March 2024

Revised: 26 April 2024

Accepted: 26 April 2024

Published: 30 April 2024



**Copyright:** © 2024 by the authors. Licensee MDPI, Basel, Switzerland. This article is an open access article distributed under the terms and conditions of the Creative Commons Attribution (CC BY) license (<https://creativecommons.org/licenses/by/4.0/>).

## 1. Introduction

Piezoelectric materials can convert mechanical energy and electrical energy into each other and are widely used in the pressure sensor, piezoelectric memory, and photovoltaic fields [1]. Piezoelectric materials have important applications in daily life technology, and the national defense industry [2].

Piezoelectric ceramic materials are mainly divided into lead and lead-free piezoelectric ceramic materials.  $Pb(Zr_xTi_{1-x})O_3$ ,  $(1-x)Pb(Mg_{1/3}Nb_{2/3})O_3-xPbTiO_3$  and other lead-containing piezoelectric materials have excellent elastic, dielectric, piezoelectric, pyroelectric, ferroelectric, electromechanical coupling and optical properties [3,4]. Therefore, they have an extremely important application value in the ultrasonic transducer, sensor, driver, filter, and memory fields. Although lead-containing piezoelectric materials are widely used because of their rich types, excellent performance and low cost [5], there is a big problem in the use of PZT-based ceramics, that is, the content of lead in its composition is more than 60%. The lead element is volatile and is a toxic substance, which brings a series of hazards to the environment and the human body in the process of use and recycling [6].

To develop new lead-free piezoelectric materials to replace PZT-based ceramics, researchers have conducted a lot of work in recent decades. At present, lead-free piezoelectric ceramic materials can be divided into five main categories: bismuth-containing layered structural materials, tungsten bronze structural materials, barium titanate ( $BaTiO_3$ , BT)-based piezoelectric materials, bismuth-sodium titanate ( $Bi_{0.5}Na_{0.5}TiO_3$ , BNT)-based piezoelectric materials and potassium sodium niobate ( $K_{1-x}Na_xNbO_3$ , KNN)-based piezoelectric materials [7]. Among them, BT, BNT, and KNN-based lead-free piezoelectric materials are perovskite structures. Due to their morphotropic phase boundary (MPB) or polycrystalline phase boundary (PPB) structures, they exhibit excellent piezoelectric properties near the

phase boundary components and have been widely studied. KNN-based ceramics have a higher Curie temperature and a lower sintering temperature than BT-based ceramics, and a higher piezoelectric constant than BNT-based ceramics, so they become the main piezoelectric materials that can replace PZT [8,9].

KNN-based ceramics have good application prospects, but their piezoelectric properties are still far inferior to PZT. At present, doping  $\text{Li}^+$  and other monovalent cations is the simplest and most efficient way to improve the piezoelectric properties [10]. Guo et al. [11] firstly reported the effect of A-position Li doping on the phase transition behavior and dielectric piezoelectric properties of KNN ceramics. They found the improved piezoelectric properties of  $d_{33} = 200\text{--}235$  pC/N when 5~7% Li was added. Song et al. [12] studied the microstructure and piezoelectric properties of KNN ceramics doped with  $\text{LiNbO}_3$  (LN), and found the best piezoelectric constant  $d_{33} = 240$  pC/N when the doping content of LN was 7%. The  $(\text{K}_{0.5}\text{Na}_{0.5})\text{NbO}_3\text{-}x\text{LiNbO}_3$  piezoelectric ceramics synthesized by Du et al. [13] showed an optimal value of  $d_{33} = 215$  pC/N when the amount of  $\text{LiNbO}_3$  was 0.06 mol. In addition, the  $(1 - x)\text{K}_{0.49}\text{Na}_{0.51}\text{NbO}_3\text{-}x\text{LiNbO}_3$  lead-free piezoelectric ceramics prepared by Shen et al. [14] also showed excellent electrical properties  $d_{33} = 246$  pC/N at  $x = 0.06$ . It was found that the doping of Li can improve the piezoelectric properties of KNN. However, it is difficult to know experimentally that Li will replace K, Na or both K and Na in the A position.

For piezoelectric materials, the excellent piezoelectric properties are mainly due to the intrinsic contribution of crystal structure (polyphase coexistence and lattice distortion) and the extrinsic contribution of microstructure (grain size and domain structure). At present, the experimental research can only explore the extrinsic contribution of its microstructure, but cannot explore the intrinsic contribution of crystal structure in more detail [15]. Therefore, this paper will study the effect of crystal structure on piezoelectric properties of materials by first-principles method. The first-principles calculation method using density functional theory (DFT) and density functional perturbation theory (DFPT) has been able to effectively support the exploration of piezoelectric properties in different crystal structures [16–18]. In our previous report, it has been shown that  $\text{LiTaO}_3$  [19] and Li [20] can improve the piezoelectric performance of  $\text{KNbO}_3$ . So, in this paper, we will further theoretically discuss the modification of Li on the structural, elastic, piezoelectric, and electronic properties of  $\text{K}_{0.5}\text{Na}_{0.5}\text{NbO}_3$ .

## 2. Calculation Methods

In this paper, the first-principles calculations were carried out by the Vienna ab initio simulation package (VASP 5.2), which is based on density functional theory and the plane-wave pseudopotential methods [21,22]. The generalized gradient approximation (GGA) and the Perdew–Burke–Ernzerhofer (PBE) exchange–correlation function were used [23,24]. The valence electron configurations considered in the calculation were K ( $3s^2 3p^6 4s^1$ ), Na ( $2s^2 2p^6 3s^1$ ), Li ( $1s^2 2s^1$ ), Nb ( $4p^6 5s^1 4d^4$ ), and O ( $2s^2 2p^4$ ), respectively. The Monkhorst–Pack k-point sampling was generated with a  $5 \times 6 \times 9$  grid for the Brillouin zone integration [25]. During the structural optimization and properties calculations, the plane wave cutoff energy of 550 eV and the energy convergence of  $10^{-7}$  eV were chosen. The structural optimization is obtained until the Hellmann–Feynman forces acting on each atom is less than  $0.005$  eV/Å. For the Born effective charge and piezoelectric stress constants calculations, the density functional perturbation theory was used [26].

## 3. Results and Discussion

### 3.1. Structural Properties

The orthogonal (Bmm2) and tetragonal (P4mm) phases of the  $\text{KNbO}_3$  primitive cell are used as the basic structure in Figure 1a,b, and 50% of K is randomly replaced by Na to construct the  $2 \times 2 \times 1$  orthogonal and  $2 \times 2 \times 2$  tetragonal of the  $\text{K}_{0.5}\text{Na}_{0.5}\text{NbO}_3$  supercell in Figure 1c,d. They are used to study the influence of different phase structures on piezoelectric properties, and the optimized lattice parameters are shown in Table 1. The calculation results in Table 1 show that the calculated values in this paper are close to other calculated values

and experimental values, and the error is less than 3%, which is within the allowable range of theory [27–29]. It can be considered that the first-principles method, related parameter settings and structural models adopted in this paper are accurate and reliable. Both the lattice parameters ( $a$ ,  $b$ ,  $c$ ) and cell volume decrease when Na is doped. This is mainly because the atomic radiuses of Na (1.91 Å) are smaller than those of K (2.35 Å).

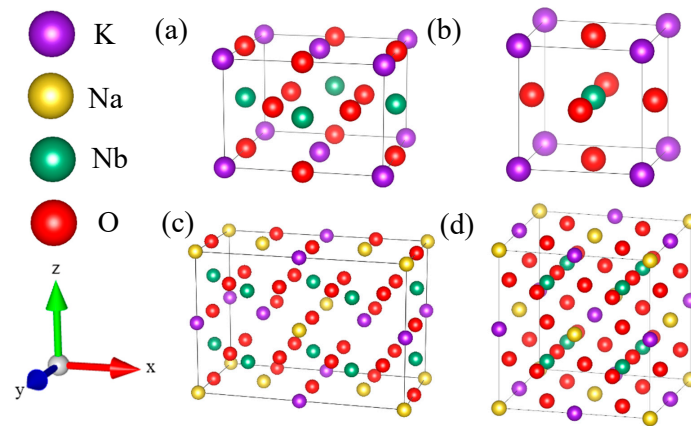


**Figure 1.** Schematic diagram of KNbO<sub>3</sub> and K<sub>0.5</sub>Na<sub>0.5</sub>NbO<sub>3</sub> crystal structure: (a) KNbO<sub>3</sub> orthogonal phase unit structure, (b) KNbO<sub>3</sub> tetragonal phase unit structure, (c) K<sub>0.5</sub>Na<sub>0.5</sub>NbO<sub>3</sub> orthogonal phase structure, and (d) K<sub>0.5</sub>Na<sub>0.5</sub>NbO<sub>3</sub> tetragonal phase structure.

**Table 1.** Lattice parameters, formation energy, piezoelectric properties ( $e_{33}$  and  $d_{33}$ ) of KNbO<sub>3</sub>, K<sub>0.5</sub>Na<sub>0.5</sub>NbO<sub>3</sub> and Li-doped K<sub>0.5-x</sub>Na<sub>0.5-y</sub>Li<sub>x+y</sub>NbO<sub>3</sub>.

Structure		$a$ (Å)	$b$ (Å)	$c$ (Å)	$V$ (Å <sup>3</sup> )	$E_f$ (eV)	$e_{33}$	$d_{33}$	
KNbO <sub>3</sub>	Orthogonal (Bmm2)	Present	5.842	4.017	5.886	138.1	/	3.00	23.74
		Calc [19]	5.832	4.020	5.869	/	/	3.02	24.5
		Calc [27]	5.789	3.991	5.822	134.5	/	/	23.25
		Expt [28]	5.697	3.971	5.721	129.4	/	/	/
	Tetragonal (P4mm)	Present	4.028	4.028	4.256	69.1	/	3.80	66.17
		Calc [27]	4.003	4.003	4.197	67.3	/	/	54.40
Expt [29]		3.996	3.996	4.063	64.9	/	/	/	
K <sub>0.5</sub> Na <sub>0.5</sub> NbO <sub>3</sub>	Orthogonal (Bmm2)	Present	5.764	3.992	5.838	134.3	/	3.96	29.15
		Expt. [30]	5.657	4	4	/	/	/	/
		Calc [27]	/	/	/	/	/	/	29.12
	Tetragonal (P4mm)	Present	4.003	4.003	4.198	67.3	/	4.81	69.44
		Calc. [31]	3.978	3.978	3.931	/	/	4.14	149
		Expt. [32]	/	/	/	/	/	/	80
$x + y = 0.06$	Expt. [33]	5.622	3.943	5.670	125.702	/	/	187	
$x + y = 0.07$	Expt. [33]	5.621	3.935	5.662	125.270	/	/	/	
K <sub>0.5-x</sub> Na <sub>0.5-y</sub> Li <sub>x+y</sub> NbO <sub>3</sub>	$x + y = 0.0625$	$x = 0.0625/y = 0$	5.659	3.937	5.700	127.0	-12.63	3.55	12.21
		$x = 0/y = 0.0625$	5.675	3.946	5.707	127.8	-12.97	5.29	24.49
	$x + y = 0.125$	$x = 0.125/y = 0$	5.635	3.916	5.691	125.6	-6.31	6.98	27.04
		$x = 0/y = 0.125$	5.684	3.949	5.708	128.1	-6.63	7.97	44.72
	$x + y = 0.25$	$x = 0.25/y = 0$	5.596	3.887	5.687	123.7	-6.42	5.10	20.33
		$x = 0/y = 0.25$	5.690	3.948	5.746	129.1	-6.85	3.72	19.58
		$x = 0.125/y = 0.125$	5.617	3.912	5.734	126.0	-6.57	4.31	23.89
	$x + y = 0.375$	$x = 0.375/y = 0$	5.592	3.839	5.651	121.3	-6.90	4.22	20.33
		$x = 0/y = 0.375$	5.701	3.962	5.765	130.2	-7.28	4.26	28.20
		$x = 0.125/y = 0.25$	5.613	3.899	5.786	126.6	-6.87	3.60	23.86
		$x = 0.25/y = 0.125$	5.605	3.898	5.696	124.5	-6.67	2.71	13.26
	$x + y = 0.5$	$x = 0.5/y = 0$	5.577	3.898	5.723	124.4	-5.75	4.19	17.97
$x = 0/y = 0.5$		5.686	3.941	5.832	130.7	-6.98	3.38	25.72	
$x = 0.125/y = 0.375$		5.653	3.926	5.752	127.7	-6.64	3.64	23.23	
$x = 0.375/y = 0.125$		5.557	3.898	5.647	122.3	-6.94	2.63	18.39	
$x = 0.25/y = 0.25$		5.667	3.933	5.723	127.6	-6.77	3.48	17.56	

To explore the properties of Li-doped  $K_{0.5}Na_{0.5}NbO_3$  ( $K_{0.5-x}Na_{0.5-y}Li_{x+y}NbO_3$ , KNN-L) at room temperature, Na or K atoms were randomly replaced by Li atoms according to the orthorhombic  $K_{0.5}Na_{0.5}NbO_3$  in Figure 1c. Different Li concentrations  $x + y$  in  $K_{0.5-x}Na_{0.5-y}Li_{x+y}NbO_3$  ( $x + y = 0.0625, 0.125, 0.25, 0.375, \text{ and } 0.5$ ) were modeled, and the optimized lattice parameters are also shown in Table 1. The results in Table 1 show that both the lattice parameters and cell volume decrease when Li is doped. The optimized lattice parameters when  $x + y = 0.0625$  are consistent with the experiment results [33] of KNN-0.06Li and KNN-0.06Li. Moreover, the lattice parameters and cell volume of structures that K replaced by Li are smaller than those of structures that Na replaced by Li. This is mainly because the atomic radiuses of Li (1.57 Å) are smaller than those of K (2.35 Å) and Na (1.91 Å).

### 3.2. Formation Energy of Doped Systems

The formation energy is the energy required when the doped element enters the crystal structure to replace the replaced element. The smaller the value, the more easily the doped element will replace the original element, and the more stable the structure of the doped system will be. For all doped systems, the formation energy can be calculated using the following expressions [34,35]:

$$E_f(K \rightarrow Li) = E(K_{0.5-x}Na_{0.5}Li_xNbO_3) - E(K_{0.5}Na_{0.5}NbO_3) + \mu_K - \mu_{Li} \quad (1)$$

$$E_f(Na \rightarrow Li) = E(K_{0.5}Na_{0.5-y}Li_yNbO_3) - E(K_{0.5}Na_{0.5}NbO_3) + \mu_{Na} - \mu_{Li} \quad (2)$$

$$E_f(K/Na \rightarrow Li) = E(K_{0.5-x}Na_{0.5-y}Li_{x+y}NbO_3) - E(K_{0.5}Nb_{0.5}O_3) + \mu_K + \mu_{Na} - \mu_{Li} \quad (3)$$

where  $E_f$  is the formation energy;  $E$  is the substituted system energy of a supercell;  $\mu$  is the chemical potential of each atom, and all the reference phases of K, Na, and Li are calculated using the structures with a  $Im\text{-}3m$  space group (No. 229).

The calculated formation energies of KNN-L are all listed in Table 1. As can be seen, the formation energies of all doped systems are negative, indicating that the structures of  $K_{0.5}Na_{0.5}NbO_3$  doped by Li atoms can exist stably. In addition, the formation energies of  $K_{0.5-x}Na_{0.5}Li_xNbO_3$  are higher than those of  $K_{0.5}Na_{0.5-y}Li_yNbO_3$ . This means that the stability of the  $K_{0.5}Na_{0.5-y}Li_yNbO_3$  structure is better, and it may be more inclined to form the  $K_{0.5}Na_{0.5-y}Li_yNbO_3$  structure in practical applications.

### 3.3. Elastic Properties

The Born stability criteria are the basis for the determination of the stability of crystal mechanics. For crystal materials, when the elastic stiffness constants conform to the Born stability criteria, the structure can be identified as stable. For orthorhombic crystal structures, the elastic stiffness matrix has nine effective values ( $C_{11}, C_{12}, C_{13}, C_{22}, C_{23}, C_{33}, C_{44}, C_{55}, C_{66}$ ), and the Born stability criteria are given as follows [36]:

$$\begin{aligned} C_{11} + C_{22} + C_{33} + 2(C_{12} + C_{13} + C_{23}) &> 0 \\ C_{11} + C_{22} &> C_{12} \\ C_{22} + C_{33} &> 2C_{23} \\ C_{11} + C_{33} &> 2C_{13} \\ C_{ij} &> 0 \quad (i, j = 1, 2, 3, 4, 5, 6) \end{aligned} \quad (4)$$

The elastic constants  $C_{ij}$  of  $K_{0.5-x}Na_{0.5-y}Li_{x+y}NbO_3$  were calculated and the results are shown in Table 2. It is shown that the elastic stiffness constants  $C_{ij}$  of all doped structures meet the Born stability criteria, that is, it can be assumed that all the doped structures with Li atoms are mechanically stable.

**Table 2.** The calculated elastic constants  $C_{ij}$  (in GPa) of  $K_{0.5-x}Na_{0.5-y}Li_{x+y}NbO_3$ .

Li Content ( $x + y$ )	$x$ and $y$	Elastic Stiffness Coefficients								
		$C_{11}$	$C_{12}$	$C_{13}$	$C_{22}$	$C_{23}$	$C_{33}$	$C_{44}$	$C_{55}$	$C_{66}$
0	Present	189.4	84.5	42.0	313.0	80.6	152.6	56.7	8.2	71.8
	Calc [27]	189.5	80.5	33.1	327.7	72.9	149.2	66.8	12.2	77.1
0.0625	$x = 0.0625/y = 0$	313.3	104.6	94.7	386.7	105.0	278.8	100.5	13.6	108.0
	$x = 0/y = 0.0625$	275.4	111.3	85.1	391.8	105.6	244.7	85.2	37.3	95.3
0.125	$x = 0.125/y = 0$	307.3	78.5	71.1	376.2	76.5	249.8	91.8	36.1	103.4
	$x = 0/y = 0.125$	280.5	110.6	82.7	399.5	110.7	239.9	57.9	48.2	83.4
0.25	$x = 0.25/y = 0$	318.7	68.9	77.1	382.6	79.2	246.9	105.4	35.8	91.3
	$x = 0/y = 0.25$	240.9	91.9	79.9	347.1	107.2	211.5	80.0	19.4	87.3
	$x = 0.125/y = 0.125$	259.1	55.2	52.9	335.3	72.8	191.9	90.3	29.5	78.8
0.375	$x = 0.375/y = 0$	285.2	65.8	64.4	343.7	54.2	200.9	92.2	49.5	82.0
	$x = 0/y = 0.375$	201.5	85.7	53.1	316.3	85.9	170.7	73.3	26.9	77.2
	$x = 0.125/y = 0.25$	239.8	55.0	48.3	314.7	79.2	170.1	84.5	20.5	70.1
	$x = 0.25/y = 0.125$	233.5	79.2	37.3	282.4	65.6	164.4	87.0	12.2	74.5
0.5	$x = 0.5/y = 0$	329.9	121.0	126.0	413.4	116.9	272.4	100.1	61.6	95.5
	$x = 0/y = 0.5$	199.9	82.1	47.0	310.2	83.1	151.2	70.8	6.6	67.7
	$x = 0.125/y = 0.375$	208.5	34.5	51.1	225.6	49.2	168.3	74.2	12.5	71.6
	$x = 0.375/y = 0.125$	133.9	39.9	3.4	144.7	16.3	147.8	80.6	42.3	85.1
	$x = 0.25/y = 0.25$	232.1	101.7	83.9	317.9	84.6	201.8	73.8	11.1	81.8

According to the calculated elastic stiffness matrix  $C_{ij}$ , the bulk modulus ( $B$ ), the shear modulus ( $G$ ), Young's modulus ( $E$ ), Poisson's ratio ( $\nu$ ), and hardness ( $G/B$ ) of all the doped systems can be calculated by the Voigt–Reuss–Hill approximation method. The upper ( $B_V$ ,  $G_V$ ) and lower ( $B_R$ ,  $G_R$ ) limits of the bulk modulus and the shear modulus, as well as the calculations of Young's modulus ( $E$ ), Poisson's ratio ( $\nu$ ), and hardness ( $G/B$ ) are given by Formulas (5)–(10) for the ortho-phase crystal structure [37,38]. The calculation results of the elastic modulus and Poisson's ratios are shown in Table 3.

$$B_V = [(C_{11} + C_{22} + C_{33}) + 2(C_{12} + C_{13} + C_{23})]/9 \quad (5)$$

$$G_V = [(C_{11} + C_{22} + C_{33} - C_{12} - C_{13} - C_{23}) + 3(C_{44} + C_{55} + C_{66})]/15 \quad (6)$$

$$B_R = 1/[(S_{11} + S_{22} + S_{33}) + 2(S_{12} + S_{13} + S_{23})] \quad (7)$$

$$G_R = 15/[4(S_{11} + S_{22} + S_{33} - S_{12} - S_{13} - S_{23}) + 3(S_{44} + S_{55} + S_{66})] \quad (8)$$

$$E = (9G \times B)/(3B + G) \quad (9)$$

$$\nu = (3B - 2G)/[2(3 \times B + G)] \quad (10)$$

**Table 3.** The calculated elastic modulus (in GPa) of  $K_{0.5-x}Na_{0.5-y}Li_{x+y}NbO_3$ .

Li Content ( $x + y$ )	$x$ and $y$	$B_V$	$B_R$	$B_H$	$G_V$	$G_R$	$G_H$	$E$	$\nu$	$G/B$
0	$x = 0/y = 0$	118.8	103.1	110.9	57.2	27.3	42.2	112.4	0.331	0.38
0.0625	$x = 0.0625/y = 0$	176.4	172.2	174.3	89.4	44.0	66.7	177.4	0.330	0.38
	$x = 0/y = 0.0625$	168.4	160.1	164.2	84.2	71.1	77.7	201.3	0.296	0.47
0.125	$x = 0.125/y = 0$	153.9	149.7	151.8	93.4	76.0	84.7	214.2	0.265	0.56
	$x = 0/y = 0.125$	169.8	159.8	164.8	79.0	63.0	71.0	186.2	0.312	0.43
0.25	$x = 0.25/y = 0$	155.4	151.5	153.4	94.7	76.0	85.3	216.0	0.265	0.56
	$x = 0/y = 0.25$	150.8	143.2	147.0	72.0	50.1	61.1	160.9	0.318	0.42
	$x = 0.125/y = 0.125$	127.6	121.1	124.3	80.1	63.2	71.6	180.3	0.258	0.58

Table 3. Cont.

Li Content ( $x + y$ )	$x$ and $y$	$B_V$	$B_R$	$B_H$	$G_V$	$G_R$	$G_H$	$E$	$\nu$	$G/B$
0.375	$x = 0.375/y = 0$	133.2	127.1	130.1	87.8	79.3	83.6	206.5	0.236	0.64
	$x = 0/y = 0.375$	126.4	111.9	119.2	66.4	53.8	60.1	154.3	0.284	0.50
	$x = 0.125/y = 0.25$	121.1	113.3	117.2	71.2	50.4	60.8	155.5	0.279	0.52
	$x = 0.25/y = 0.125$	116.1	107.0	111.5	67.9	37.8	52.9	137.0	0.295	0.47
0.5	$x = 0.5/y = 0$	193.7	189.1	191.4	94.9	89.1	92.0	237.9	0.293	0.48
	$x = 0/y = 0.5$	120.6	106.2	113.4	59.0	23.8	41.4	110.6	0.337	0.36
	$x = 0.125/y = 0.375$	96.9	88.4	92.7	62.8	34.0	48.4	123.7	0.278	0.52
	$x = 0.375/y = 0.125$	60.6	59.1	59.9	66.0	60.7	63.4	140.5	0.109	1.06
	$x = 0.25/y = 0.25$	143.6	137.9	140.8	65.5	35.2	50.3	134.8	0.340	0.36

As can be seen from Table 3, the bulk modulus, the shear modulus, and Young's modulus of KNN-L are mostly higher than those of KNN, and the hardness value increases. The Poisson ratio of KNN-L is lower than that of most KNN, and the ductility is reduced. The  $B_H$  of  $K_{0.5-x}Na_{0.5}Li_xNbO_3$  is greater than that of  $K_{0.5}Na_{0.5-y}Li_yNbO_3$  except for  $x = 0.125$ . When Li is doped in a small amount ( $x = 0.0625$ ), the  $\nu$  of  $K_{0.5-x}Na_{0.5}Li_xNbO_3$  is greater than that of  $K_{0.5}Na_{0.5-y}Li_yNbO_3$ , and the  $G_H$ ,  $E$  and  $G/B$  of  $K_{0.5-x}Na_{0.5}Li_xNbO_3$  are smaller than the those of  $K_{0.5}Na_{0.5-y}Li_yNbO_3$ . However, when the doping amount of Li is increased ( $x = 0.125, 0.25, 0.375, 0.5$ ), the  $\nu$  of  $K_{0.5-x}Na_{0.5}Li_xNbO_3$  is less than that of  $K_{0.5}Na_{0.5-y}Li_yNbO_3$ , and the  $G_H$ ,  $E$  and  $G/B$  of  $K_{0.5-x}Na_{0.5}Li_xNbO_3$  are greater than those of  $K_{0.5}Na_{0.5-y}Li_yNbO_3$ . This means that  $K_{0.5-x}Na_{0.5}Li_xNbO_3$  is harder and less ductile than  $K_{0.5}Na_{0.5-y}Li_yNbO_3$ .

The three-dimensional curves of Young's modulus are drawn according to the elastic modulus data, as shown in Figures 2 and 3. The greater the difference between the 3D curves and the 3D sphere, the stronger the anisotropy of the material. Comparing  $K_{0.5}Na_{0.5}NbO_3$  in Figure 2a, it can be observed from Figure 2b–f that the 3D curves of Young's modulus of the  $K_{0.5-x}Na_{0.5}Li_xNbO_3$  structure are significantly less deviated from the sphere, indicating that the incorporation of Li atoms makes  $K_{0.5-x}Na_{0.5}Li_xNbO_3$  less anisotropic.

In the  $K_{0.5}Na_{0.5-y}Li_yNbO_3$  system, comparing  $K_{0.5}Na_{0.5}NbO_3$  in Figure 3a, the anisotropy of Young's modulus of Figure 3c ( $y = 0.125$ ) and Figure 3f ( $y = 0.5$ ) increase, while the anisotropy of doped structures in Figure 3b,d,e decrease.

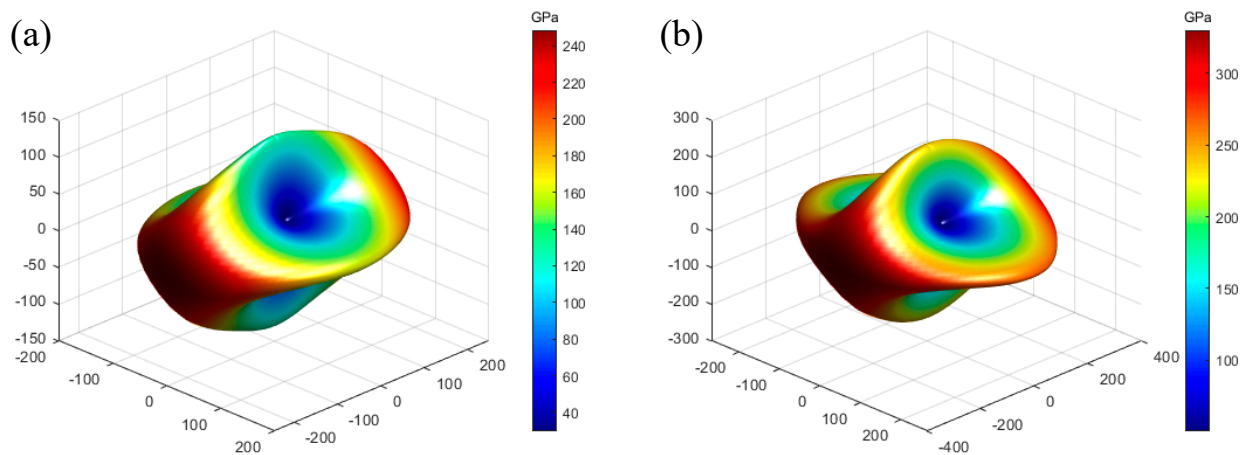
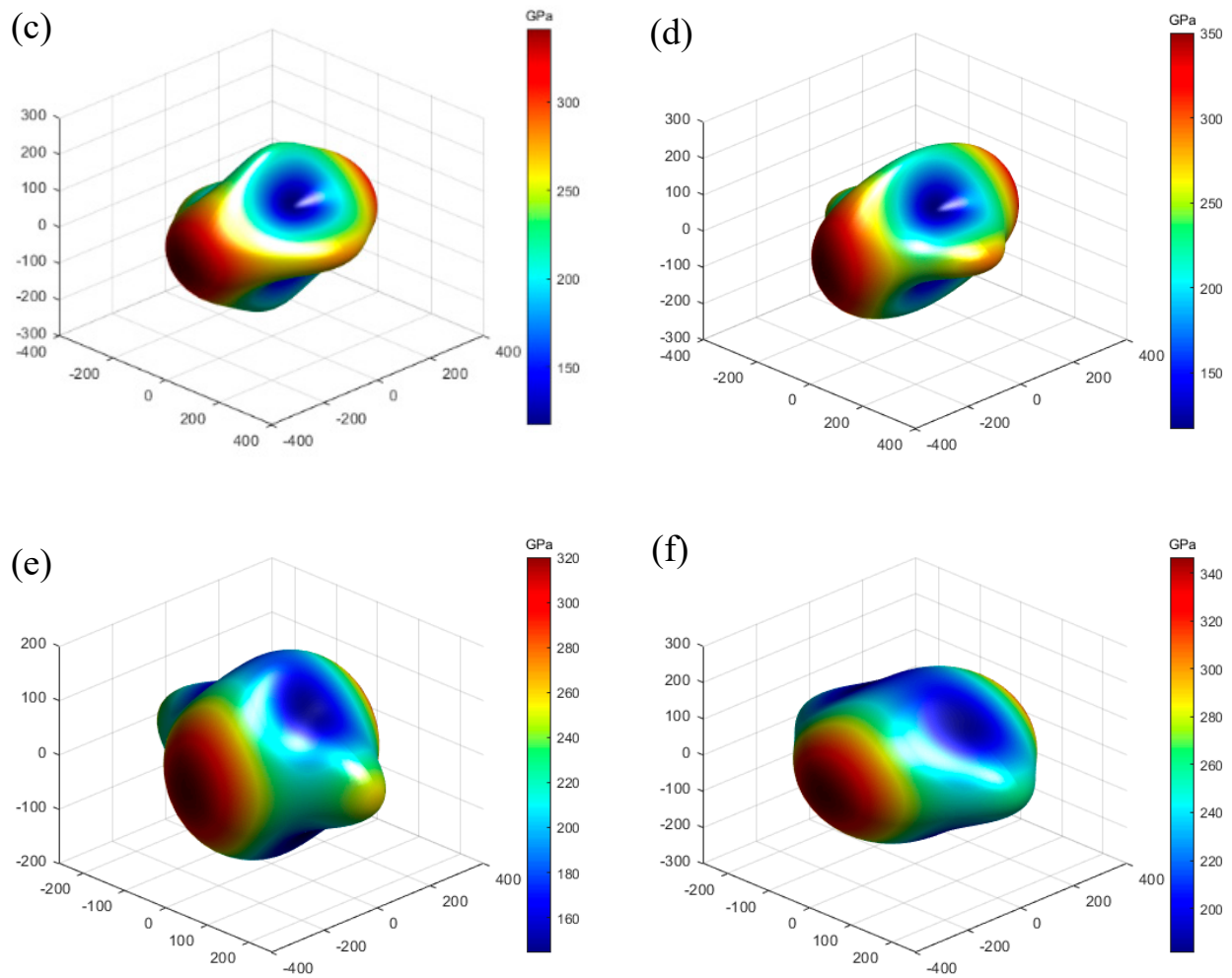
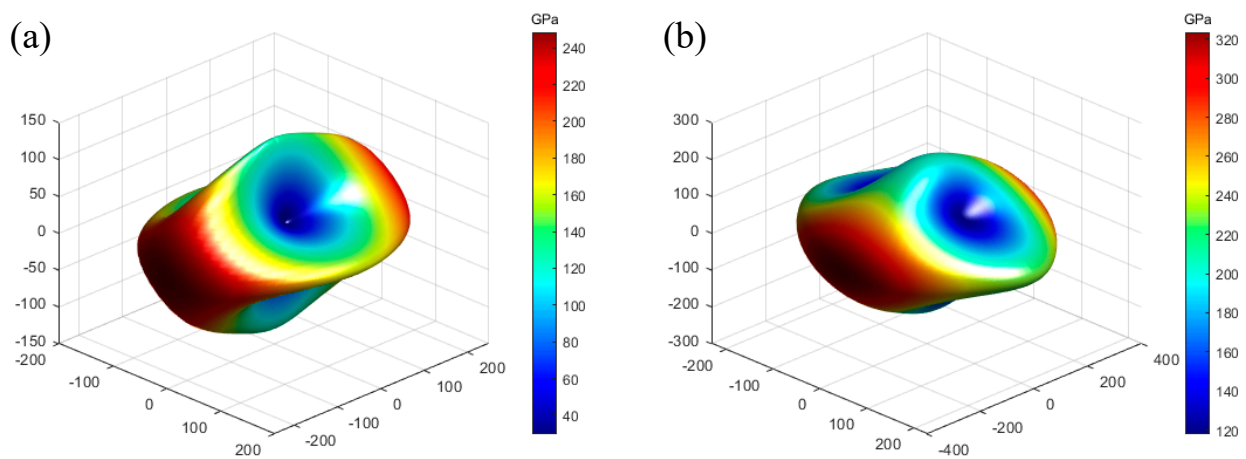


Figure 2. Cont.



**Figure 2.** Three-dimensional curves of Young's modulus  $E$  (in GPa) for Li doping K in  $K_{0.5-x}Na_{0.5}Li_xNbO_3$ : (a)  $x = 0$ , (b)  $x = 0.0625$ , (c)  $x = 0.125$ , (d)  $x = 0.25$ , (e)  $x = 0.375$ , and (f)  $x = 0.5$ .



**Figure 3.** Cont.

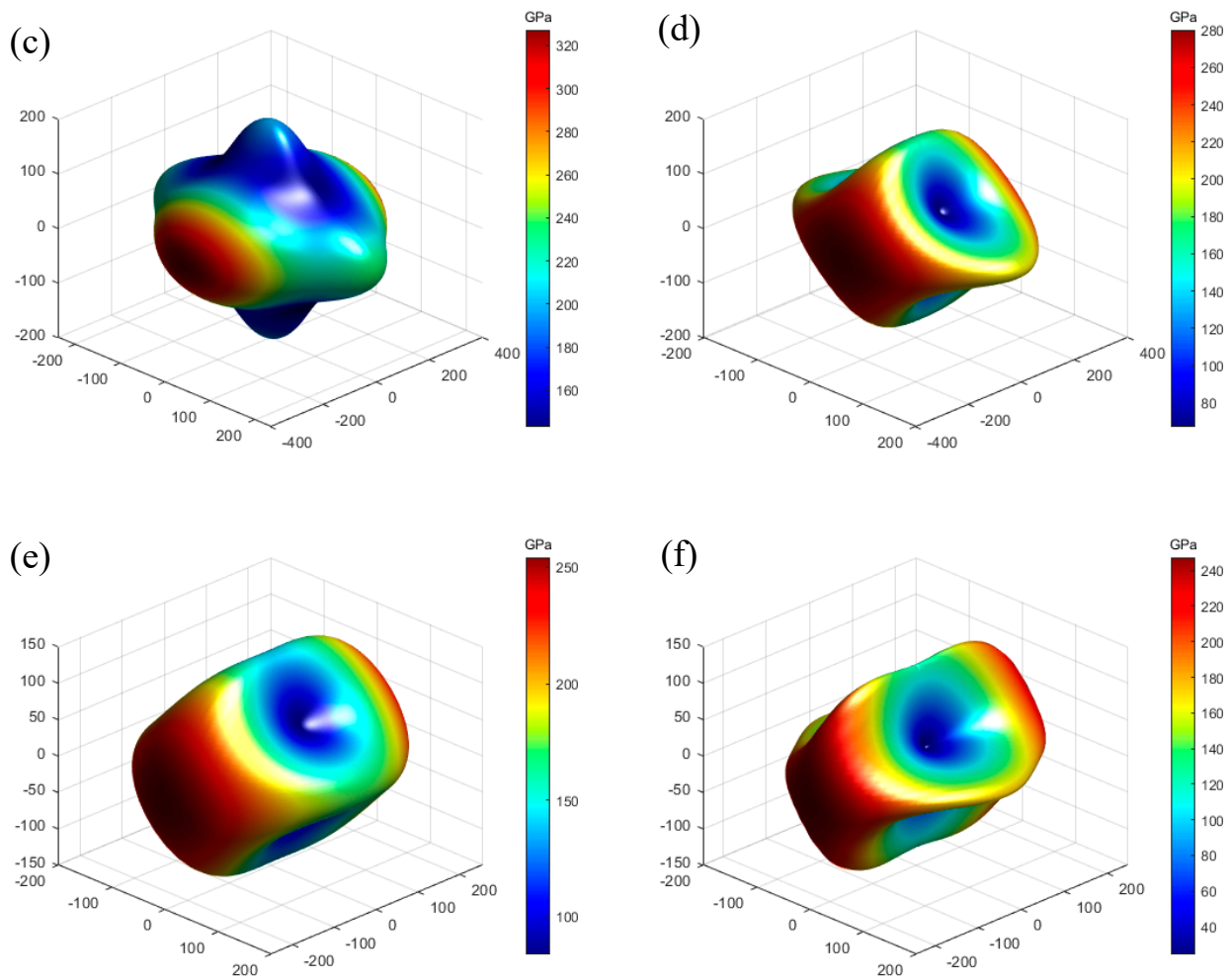


**Figure 3.** Three-dimensional curves of Young's modulus  $E$  (in GPa) for Li doping Na in  $K_{0.5}Na_{0.5-y}Li_yNbO_3$ : (a)  $y = 0$ , (b)  $y = 0.0625$ , (c)  $y = 0.125$ , (d)  $y = 0.25$ , (e)  $y = 0.375$ , and (f)  $y = 0.5$ .

### 3.4. Piezoelectric Properties

In the perovskite material system, there is a linear coupling relationship between mechanical properties and electrical properties. The piezoelectric constant describing the linear relationship between force and electricity calculation formula is as follows [39]:

$$d_{\alpha j} = \sum_{i=1}^6 e_{\alpha i} S_{ij} \quad (11)$$

where  $d_{\alpha j}$  refers to the piezoelectric charge tensor,  $\alpha = 1-3$  and  $j = 1-6$ ;  $e_{\alpha i}$  is the piezoelectric stress tensor,  $i = 1-6$ ; and  $S_{ij}$  is the elastic compliance coefficient. Since  $d_{\alpha j}$  and  $e_{\alpha i}$  are  $3 \times 6$  matrices and  $S_{ij}$  is  $6 \times 6$  matrices, we use  $\alpha$ ,  $i$ , and  $j$  to distinguish the rows and columns. In the piezoelectric charge tensor  $d_{\alpha j}$ ,  $d_{33}$  is the most commonly used piezoelectric constant to characterize the performance of a piezoelectric material.

The  $e_{33}$  and  $d_{33}$  of  $KNbO_3$  and  $K_{0.5-x}Na_{0.5-y}Li_{x+y}NbO_3$  are also shown in Table 1. The  $d_{33}$  of  $KNbO_3$  and  $K_{0.5}Na_{0.5}NbO_3$  tetragonal phase are higher than that of  $KNbO_3$  and  $K_{0.5}Na_{0.5}NbO_3$  orthogonal phase. It can be inferred that the excellent piezoelectric properties in the polyphase coexisting region, explained from the aspect of crystal structure, may be due to the tetragonal phase with good piezoelectric properties compensating for the orthogonal phase with poor piezoelectric properties. In addition, the  $d_{33}$  of  $K_{0.5-x}Na_{0.5-y}Li_{x+y}NbO_3$  reached the maximum value (44.72 pC/N) when  $x = 0.125$ , and compared with the  $d_{33}$  of  $K_{0.5}Na_{0.5}NbO_3$  (29.15 pC/N), it is 1.5-fold higher. In order to

more clearly reflect the variation trend of  $d_{33}$  with Li content, Figure 4 was plotted with all the  $d_{33}$  values (blue dots) of  $\text{K}_{0.5-x}\text{Na}_{0.5-y}\text{Li}_{x+y}\text{NbO}_3$  in Table 1. As shown in Figure 4, the maximum  $d_{33}$  (solid red line) for each Li content first increased and then decreased with the increase in Li, which is consistent with the experimental results.

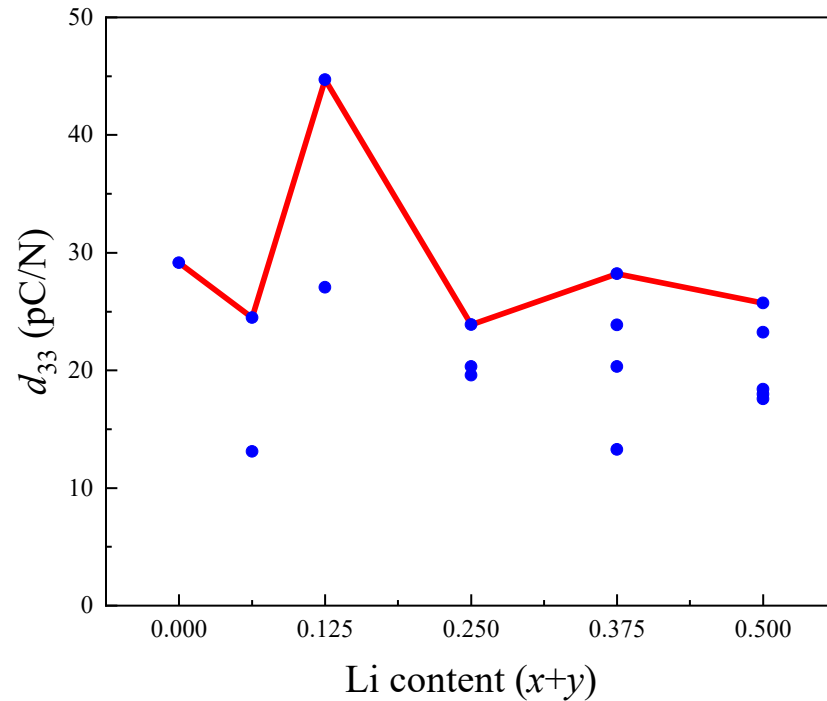


**Figure 4.** The piezoelectric charge tensor  $d_{33}$  of KNN-L with different Li content.

### 3.5. The Born Effective Charge

In piezoelectric materials with perovskite structure, a larger Born effective charge tends to generate a larger spontaneous field. For piezoelectric materials, the greater the spontaneous polarization, the better the piezoelectric characteristics. Usually, the Born effective charge ( $Z^*$ ) can be obtained by using the following equation [40]:

$$P_{\alpha} = \frac{e}{\Omega} \sum Z_{i\alpha\beta}^* \delta_{ui\beta} \quad (12)$$

where  $P_{\alpha}$  means the macroscopic polarization;  $i, \alpha, \beta$  represent the  $i$ -th atom, the direction of the polarization component, and atomic displacement, respectively;  $\delta_u$  represents the atomic displacement.

To investigate the effect of Li doped on piezoelectric properties, the Born effective charges of  $\text{KNbO}_3$ ,  $\text{K}_{0.5}\text{Na}_{0.5}\text{NbO}_3$  and  $\text{K}_{0.5}\text{Na}_{0.375}\text{Li}_{0.125}\text{NbO}_3$  are calculated by the DFPT method, and the results are shown in Table 4. As can be seen from Table 4, due to the addition of Li, the  $\bar{Z}^*$  of Nb and  $\text{O}_I$  atoms in  $\text{K}_{0.5}\text{Na}_{0.375}\text{Li}_{0.125}\text{NbO}_3$  structure increase compared with those in  $\text{KNbO}_3$  and  $\text{K}_{0.5}\text{Na}_{0.5}\text{NbO}_3$ . This is also consistent with the calculated results of piezoelectric properties.

**Table 4.** The Born effective charge of  $\text{KNbO}_3$ ,  $\text{K}_{0.5}\text{Na}_{0.5}\text{NbO}_3$  and  $\text{K}_{0.5}\text{Na}_{0.375}\text{Li}_{0.125}\text{NbO}_3$ .

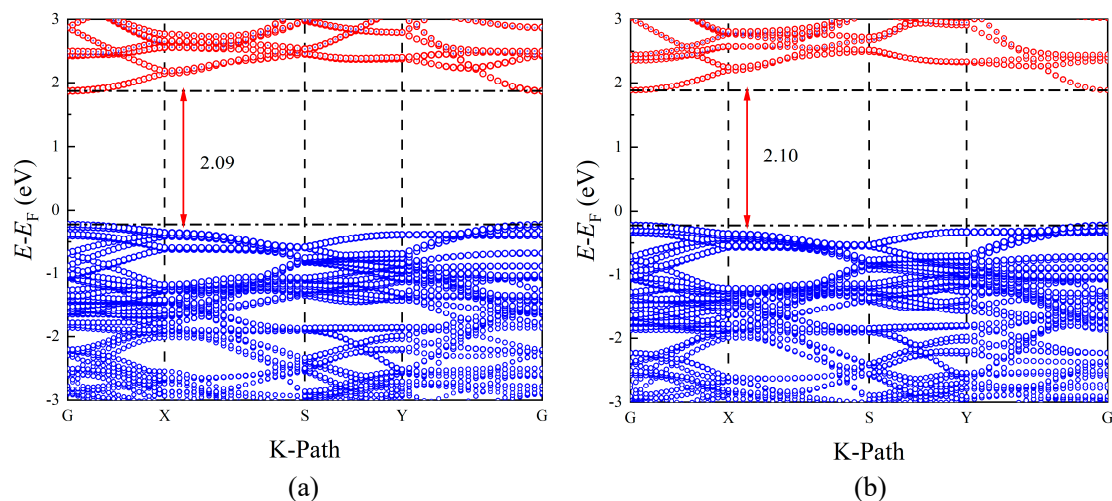
Materials	Species	$Z_{xx}^*$	$Z_{yy}^*$	$Z_{zz}^*$	$\bar{Z}^*$
KN	K	1.208	1.135	1.177	1.173
	Nb	7.454	8.836	6.243	7.511
	$\text{O}_I$	-1.354	-6.915	-1.437	-3.236
	$\text{O}_{II}$	-3.654	-1.528	-2.992	-2.724

Table 4. Cont.

Materials	Species	$Z_{xx}^*$	$Z_{yy}^*$	$Z_{zz}^*$	$\bar{Z}^*$
KNN	K	1.169	1.150	1.170	1.163
	Na	1.234	1.142	1.140	1.172
	Nb	7.664	8.740	6.473	7.625
	O <sub>I</sub>	−1.378	−7.068	−1.430	−3.292
	O <sub>II</sub>	−3.779	−1.469	−3.117	−2.788
KNN-L	K	1.179	1.076	1.152	1.136
	Na	1.342	1.324	1.320	1.329
	Li	1.067	1.056	0.993	1.039
	Nb	7.888	8.739	7.260	7.962
	O <sub>I</sub>	−1.513	−7.087	−1.504	−3.368
	O <sub>II</sub>	−3.444	−1.476	−3.234	−2.718

### 3.6. Band Structure

The band structures are shown in Figure 5. In order to calculate the band, the high-symmetry point path of G-X-S-Y-G is used. As can be seen from Figure 5,  $K_{0.5}Na_{0.5}NbO_3$  and  $K_{0.5}Na_{0.375}Li_{0.125}NbO_3$  are all the direct band gap semiconductors, and the valence band maximum (VBM) and the conduction band minimum (CBM) are all located at the highly symmetric G-point. A direct band gap semiconductor has better energy utilization and electrical performance because its electrons will directly transition to a conduction band from a valence band when excited. In addition, the calculations show that the direct band gap of 2.09 eV for  $K_{0.5}Na_{0.5}NbO_3$  (comparable to the calculated result of 2.21 eV [31] and experiment value of 3.11 eV [41]) and 2.10 eV for  $K_{0.5}Na_{0.375}Li_{0.125}NbO_3$  (1.96 eV [31]) is not much different. Li makes the CBM (1.87 to 1.88 eV) of  $K_{0.5}Na_{0.375}Li_{0.125}NbO_3$  slightly move towards the higher energy level, and VBM (−0.22 eV) of  $K_{0.5}Na_{0.375}Li_{0.125}NbO_3$  is consistent with  $K_{0.5}Na_{0.5}NbO_3$ .



**Figure 5.** Band structures of undoped and Li-doped KNN: (a)  $K_{0.5}Na_{0.5}NbO_3$  and (b)  $K_{0.5}Na_{0.375}Li_{0.125}NbO_3$ . (The red line is Nb contributing band, and the blue line is O contributing band).

### 3.7. Density of States

The total and partial density of states (DOS and PDOS) of  $K_{0.5}Na_{0.5}NbO_3$  and  $K_{0.5}Na_{0.375}Li_{0.125}NbO_3$  are calculated, and the calculation results are shown in Figure 6. The DOS main peaks of  $K_{0.5}Na_{0.375}Li_{0.125}NbO_3$  are mainly concentrated in four regions (−17~−15 eV, −12~−10 eV, −5~0 eV, 2~7 eV), which are similar to those of  $K_{0.5}Na_{0.5}NbO_3$ .

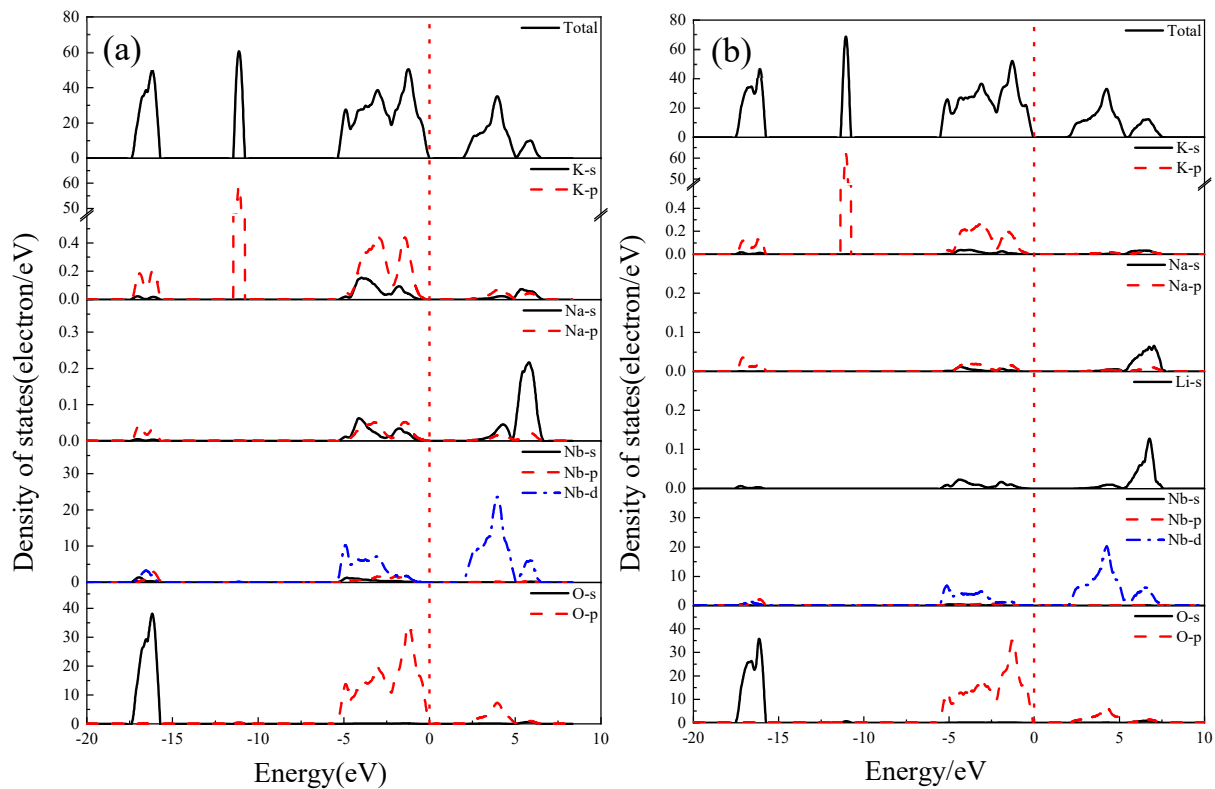


**Figure 6.** DOS and PDOS of undoped and Li-doped KNN: (a)  $\text{K}_{0.5}\text{Na}_{0.5}\text{NbO}_3$  and (b)  $\text{K}_{0.5}\text{Na}_{0.375}\text{Li}_{0.125}\text{NbO}_3$ .

For the  $\text{K}_{0.5}\text{Na}_{0.375}\text{Li}_{0.125}\text{NbO}_3$  structure in Figure 6b, the valence band ( $-5\sim 0$  eV) near the Fermi surface is mainly composed of s and p orbitals of K, Na and Li, O-2p, and Nb-4d orbitals. Similar to  $\text{K}_{0.5}\text{Na}_{0.5}\text{NbO}_3$ , the component of the conduction band is also contributed by O-2p and Nb-4d orbitals. However, compared with  $\text{K}_{0.5}\text{Na}_{0.5}\text{NbO}_3$ , Li reduces the contribution of K and Na to the valence band and conduction band, making the peak shape sharp and the conduction band move towards a higher energy level. This indicates that the Li has a strong effect on the electronic structure of  $\text{K}_{0.5}\text{Na}_{0.5}\text{NbO}_3$ .

#### 4. Conclusions

In this paper, the structural, elastic, piezoelectric, and electronic properties of Li-doped  $\text{K}_{0.5-x}\text{Na}_{0.5-y}\text{Li}_{x+y}\text{NbO}_3$  were calculated using VASP software. The influence of different proportions of KNN-L was explored. The results show that the properties of KNN-L are related to the Li-doping content and the replaced K or Na atoms. The stability of the Na-replaced  $\text{K}_{0.5}\text{Na}_{0.5-y}\text{Li}_y\text{NbO}_3$  structure is better than that of the K-replaced  $\text{K}_{0.5-x}\text{Na}_{0.5}\text{Li}_x\text{NbO}_3$ , and it may be more inclined to form the  $\text{K}_{0.5}\text{Na}_{0.5-y}\text{Li}_y\text{NbO}_3$  structure in experiments. The bulk modulus, the shear modulus and Young's modulus of KNN-L are mostly higher than those of KNN, and the hardness value increases. The Poisson ratio of KNN-L is lower than that of most KNN, and the ductility is reduced. The incorporation of Li atoms makes  $\text{K}_{0.5-x}\text{Na}_{0.5}\text{Li}_x\text{NbO}_3$  less anisotropic, but the anisotropy of  $\text{K}_{0.5}\text{Na}_{0.5-y}\text{Li}_y\text{NbO}_3$  decreases first and then increases with the addition of Li atoms. All doped systems are direct band gap semiconductors. The band gaps of  $\text{K}_{0.5}\text{Na}_{0.5}\text{NbO}_3$  (2.09 eV) and  $\text{K}_{0.5}\text{Na}_{0.375}\text{Li}_{0.125}\text{NbO}_3$  (2.10 eV) are similar. Among the Li-doped KNN-L structures,  $\text{K}_{0.5}\text{Na}_{0.375}\text{Li}_{0.125}\text{NbO}_3$  has the largest piezoelectric charge constant,  $d_{33} = 44.72$  pC/N, which is 1.5 fold that of  $\text{K}_{0.5}\text{Na}_{0.5}\text{NbO}_3$  (29.15 pC/N). The results show that the Li-doped  $\text{K}_{0.5}\text{Na}_{0.5}\text{NbO}_3$  system helps to improve its piezoelectric capacity.

**Author Contributions:** H.L., methodology, software, investigation, conceptualization, writing—review and editing, visualization, supervision and funding acquisition; T.Z., validation, formal analysis, investigation, data curation, and writing—original draft preparation; K.X., investigation and writing—original draft preparation; H.W., investigation and writing—review and editing; W.L., investigation and writing—review and editing; J.L., investigation and writing—review and editing. All authors have read and agreed to the published version of the manuscript.

**Funding:** This research was funded by the Fundamental Research Funds for the Central Universities, CHD (Nos. 300102312406, 300102312405).

**Institutional Review Board Statement:** Not applicable.

**Informed Consent Statement:** Not applicable.

**Data Availability Statement:** Data are contained within this article.

**Acknowledgments:** The authors also acknowledge the Northwestern Polytechnical University High Performance Computing Center for the allocation of computing time on their machines.

**Conflicts of Interest:** The authors declare no conflicts of interest.

## References

1. Zheng, T.; Wu, J.; Xiao, D.; Zhu, J. Recent development in lead-free perovskite piezoelectric bulk materials. *Prog. Mater. Sci.* **2018**, *98*, 552–624. [[CrossRef](#)]
2. Yang, Z.; Du, H.; Jin, L.; Poelman, D. High-performance lead-free bulk ceramics for electrical energy storage applications: Design strategies and challenges. *J. Mater. Chem. A* **2021**, *9*, 18026–18085. [[CrossRef](#)]
3. Yang, L.; Kong, X.; Li, F.; Hao, H.; Cheng, Z.; Liu, H.; Li, J.F.; Zhang, S. Perovskite lead-free dielectrics for energy storage applications. *Prog. Mater. Sci.* **2019**, *102*, 72–108. [[CrossRef](#)]
4. Xu, K.; Li, J.; Lv, X.; Wu, J.; Zhang, X.; Xiao, D.; Zhu, J. Superior piezoelectric properties in potassium–sodium niobate lead-free ceramics. *Adv. Mater.* **2016**, *28*, 8519–8523. [[CrossRef](#)]
5. Jie, X.; Zhi, T.; Ting, Z.; Jia-Gang, W.; Ding-Quan, X.; Jian-Guo, Z. Research progress of high piezoelectric activity of potassium sodium niobate based lead-free ceramics. *Acta Phys. Sin.* **2020**, *69*, 19.
6. Wu, B.; Wu, H.; Wu, J.; Xiao, D.; Zhu, J.; Pennycook, S.J. Giant piezoelectricity and high Curie temperature in nanostructured alkali niobate lead-free piezoceramics through phase coexistence. *J. Am. Chem. Soc.* **2016**, *138*, 15459–15464. [[CrossRef](#)]
7. Panda, P.K.; Sahoo, B.; Thejas, T.S.; Krishna, M. High  $d_{33}$  lead-free piezoceramics: A Review. *J. Electron. Mater.* **2022**, *51*, 938–952. [[CrossRef](#)]
8. Panda, P.K.; Sahoo, B. PZT to Lead Free Piezo Ceramics: A Review. *Ferroelectrics* **2015**, *474*, 128–143. [[CrossRef](#)]
9. Lv, X.; Zhu, J.; Xiao, D.; Zhang, X.X.; Wu, J. Emerging new phase boundary in potassium sodium-niobate based ceramics. *Chem. Soc. Rev.* **2020**, *49*, 671–707. [[CrossRef](#)] [[PubMed](#)]
10. Zhao, Y.; Ge, Y.; Zhang, X.; Zhao, Y.; Zhou, H.; Li, J.; Jin, H. Comprehensive investigation of  $\text{Er}_2\text{O}_3$  doped  $(\text{Li}, \text{K}, \text{Na})\text{NbO}_3$  ceramics rendering potential application in novel multifunctional devices. *J. Alloy. Compd.* **2016**, *683*, 171–177. [[CrossRef](#)]
11. Guo, Y.; Kakimoto, K.I.; Ohsato, H. Phase transitional behavior and piezoelectric properties of  $(\text{Na}_{0.5}\text{K}_{0.5})\text{NbO}_3$ - $\text{LiNbO}_3$  ceramics. *Appl. Phys. Lett.* **2004**, *85*, 4121–4123. [[CrossRef](#)]
12. Song, H.C.; Cho, K.H.; Park, H.Y.; Ahn, C.W.; Nahm, S.; Uchino, K.; Park, S.H.; Lee, H.G. Microstructure and piezoelectric properties of  $(1-x)(\text{Na}_{0.5}\text{K}_{0.5})\text{NbO}_3$ - $x\text{LiNbO}_3$  Ceramics. *J. Am. Ceram. Soc.* **2007**, *90*, 1812–1816. [[CrossRef](#)]
13. Du, H.; Tang, F.; Liu, D.; Zhu, D.; Zhou, W.; Qu, S. The microstructure and ferroelectric properties of  $(\text{K}_{0.5}\text{Na}_{0.5})\text{NbO}_3$ - $\text{LiNbO}_3$  lead-free piezoelectric ceramics. *Mater. Sci. Eng. B* **2007**, *136*, 165–169. [[CrossRef](#)]
14. Shen, Z.Y.; Li, Y.M.; Jiang, L.; Li, R.R.; Wang, Z.M.; Hong, Y.; Liao, R.H. Phase transition and electrical properties of  $\text{LiNbO}_3$ -modified  $\text{K}_{0.49}\text{Na}_{0.51}\text{NbO}_3$  lead-free piezoceramics. *J. Mater. Sci.-Mater. Electron.* **2011**, *22*, 1071–1075. [[CrossRef](#)]
15. Hao, J.; Li, W.; Zhai, J.; Chen, H. Progress in high-strain perovskite piezoelectric ceramics. *Mater. Sci. Eng. R-Rep.* **2019**, *135*, 1–57. [[CrossRef](#)]
16. Machado, R.; Sepliarsky, M.; Stachiotti, M.G. Relative phase stability and lattice dynamics of  $\text{NaNbO}_3$  from first-principles calculations. *Phys. Rev. B* **2011**, *84*, 134107. [[CrossRef](#)]
17. Xu, Y.Q.; Wu, S.Y.; Zhang, L.J.; Wu, L.N.; Ding, C.C. First-principles study of structural, electronic, elastic, and optical properties of cubic  $\text{KNbO}_3$  and  $\text{KTaO}_3$  crystals. *Phys. Status Solidi B* **2017**, *254*, 1600620. [[CrossRef](#)]
18. Zhou, S.L.; Zhao, X.; Jiang, X.P.; Han, X.D. Electronic and optical properties of  $\text{KNbO}_3$ ,  $\text{NaNbO}_3$  and  $\text{K}_{0.5}\text{Na}_{0.5}\text{NbO}_3$  in paraelectric cubic phase: A comparative first-principles study. *Chin. J. Struct. Chem.* **2012**, *31*, 1095–1104.
19. Li, H.; Wang, L.; Xu, L.; Li, A.; Mao, P.; Wu, Q.; Xie, Z. First-principles study on the structural, elastic, piezoelectric and electronic properties of  $(\text{BaTiO}_3, \text{LiTaO}_3)$ -modified  $\text{KNbO}_3$ . *Mater. Today Commun.* **2021**, *26*, 102092. [[CrossRef](#)]
20. Li, H.; Wu, Q.; Zhou, T.; Wang, Y.; Qiu, Y.; Xu, K.; Zhao, X.; He, Z.; Yu, P. Elastic, piezoelectric, and electronic properties of  $\text{K}_{1-x}\text{M}_x\text{NbO}_3$  ( $\text{M} = \text{Li}, \text{Na}$ ): A first-principles study. *AIP Adv.* **2023**, *13*, 075012. [[CrossRef](#)]

21. Kresse, G. Efficient iterative schemes for ab initio total-energy calculations using a plane-wave basis set. *Phys. Rev. B* **1996**, *54*, 11169. [[CrossRef](#)] [[PubMed](#)]
22. Kresse, G.; Hafner, J. Ab initio molecular dynamics for open-shell transition metals. *Phys. Rev. B* **1993**, *48*, 13115–13118. [[CrossRef](#)] [[PubMed](#)]
23. Blöchl, P. Projector augmented-wave method. *Phys. Rev. B* **1994**, *50*, 17953–17979. [[CrossRef](#)] [[PubMed](#)]
24. Perdew, J.P.; Burke, K.; Ernzerhof, M. Generalized gradient approximation made simple. *Phys. Rev. Lett.* **1996**, *77*, 3865–3868. [[CrossRef](#)] [[PubMed](#)]
25. Monkhorst, H.J.; Pack, J.D. Special points for Brillouin-zone integrations. *Phys. Rev. B* **1976**, *13*, 5188–5192. [[CrossRef](#)]
26. Gonze, X.; Lee, C. Dynamical matrices, Born effective charges, dielectric permittivity tensors, and interatomic force constants from density-functional perturbation theory. *Phys. Rev. B* **1997**, *55*, 10355–10368. [[CrossRef](#)]
27. Peng, Y.; Tan, Z.; An, J.; Zhu, J.; Zhang, Q. The tunable ferroelectricity and piezoelectricity of the KNN piezoceramics by Na concentrations: First-principles calculations. *J. Eur. Ceram. Soc.* **2019**, *39*, 5252–5259. [[CrossRef](#)]
28. Katz, L.; Megaw, H.J.A.C. The structure of potassium niobate at room temperature: The solution of a pseudosymmetric structure by Fourier methods. *Acta Crystallogr.* **1967**, *22*, 639–648. [[CrossRef](#)]
29. Hewat, A.W. Cubic-tetragonal-orthorhombic-rhombohedral ferroelectric transitions in perovskite potassium niobate: Neutron powder profile refinement of the structures. *J. Phys. C Solid State Phys.* **1973**, *6*, 2559. [[CrossRef](#)]
30. Wang, Q.; Han, Y.; Liu, C.; Ma, Y.; Ren, W.; Gao, C. High-pressure electrical transport properties of KNbO<sub>3</sub>, Experimental and theoretical approaches. *Appl. Phys. Lett.* **2012**, *100*, 172905. [[CrossRef](#)]
31. Hill, R. The elastic behaviour of a crystalline aggregate. *Proc. Phys. Soc.* **1952**, *65*, 349–354. [[CrossRef](#)]
32. Kosec, M.; Bobnar, V.; Hrovat, M.; Bernard, J.; Malic, B.; Holc, J. New lead-free relaxors based on the K<sub>0.5</sub>Na<sub>0.5</sub>NbO<sub>3</sub>-SrTiO<sub>3</sub> solid solution. *J. Mater. Res.* **2004**, *19*, 1849–1854. [[CrossRef](#)]
33. Tellier, J.; Malic, B.; Dkhil, B.; Jenko, D.; Cilensek, J.; Kosec, M. Crystal structure and phase transitions of sodium potassium niobate perovskites. *Solid State Sci.* **2009**, *11*, 320–324. [[CrossRef](#)]
34. Yang, D.; Wei, L.L.; Chao, X.L.; Yang, Z.P.; Zhou, X.Y. First-principles calculation of the effects of Li-doping on the structure and piezoelectricity of (K<sub>0.5</sub>Na<sub>0.5</sub>)NbO<sub>3</sub> lead-free ceramics. *Phys. Chem. Chem. Phys.* **2016**, *18*, 7702–7706. [[CrossRef](#)]
35. Egerton, L.; Dillon, D.M. Piezoelectric and dielectric properties of ceramics in the system potassium-sodium niobate. *J. Am. Ceram. Soc.* **1959**, *42*, 438–442. [[CrossRef](#)]
36. Long, C.; Li, T.; Fan, H.; Wu, Y.; Zhou, L.; Li, Y.; Xiao, L.; Li, Y. Li-substituted K<sub>0.5</sub>Na<sub>0.5</sub>NbO<sub>3</sub>-based piezoelectric ceramics: Crystal structures and the effect of atmosphere on electrical properties. *J. Alloys Compd.* **2016**, *658*, 839–847. [[CrossRef](#)]
37. Choi, M.; Oba, F.; Tanaka, I. First-principles study of native defects and lanthanum impurities in NaTaO<sub>3</sub>. *Phys. Rev. B* **2008**, *78*, 014115. [[CrossRef](#)]
38. Li, C.; Xu, X.; Gao, Q.; Lu, Z. First-principle calculations of the effects of CaZrO<sub>3</sub>-doped on the structure of KNN lead-free ceramics. *Ceram. Int.* **2019**, *45*, 11092–11098. [[CrossRef](#)]
39. Mouhat, F.; Coudert, F.-X. Necessary and sufficient elastic stability conditions in various crystal systems. *Phys. Rev. B* **2014**, *90*, 224104. [[CrossRef](#)]
40. Li, F.; Zhang, S.; Xu, Z.; Wei, X.; Luo, J.; ShROUT, T.R. Investigation of electromechanical properties and related temperature characteristics in domain-engineered tetragonal Pb(In<sub>1/2</sub>Nb<sub>1/2</sub>)O<sub>3</sub>-Pb(Mg<sub>1/3</sub>Nb<sub>2/3</sub>)O<sub>3</sub>-PbTiO<sub>3</sub> crystals. *J. Am. Ceram. Soc.* **2010**, *93*, 2731–2734. [[CrossRef](#)]
41. Zgonik, M.; Bernasconi, P.; Duelli, M.; Schlessner, R.; Günter, P.; Garrett, M.H.; Rytz, D.; Zhu, Y.; Wu, X. Dielectric, elastic, piezoelectric, electro-optic, and elasto-optic tensors of BaTiO<sub>3</sub> crystals. *Phys. Rev. B* **1994**, *50*, 5941. [[CrossRef](#)] [[PubMed](#)]

**Disclaimer/Publisher's Note:** The statements, opinions and data contained in all publications are solely those of the individual author(s) and contributor(s) and not of MDPI and/or the editor(s). MDPI and/or the editor(s) disclaim responsibility for any injury to people or property resulting from any ideas, methods, instructions or products referred to in the content.